Nanoscale Research Letters

NANO EXPRESS Open Access

Adsorption of Cadmium Ions from an Aqueous Solution on a Highly Stable Dopamine-Modified Magnetic Nano-Adsorbent

Ting Lei, Sheng-Jian Li, Fang Jiang, Zi-Xuan Ren, Li-Lian Wang, Xiang-Jun Yang, Li-Hong Tang* and Shi-Xiong Wang*

Abstract

Magnetic nanomaterials were functionalized with dopamine hydrochloride as the functional reagent to afford a core–shell-type Fe_3O_4 modified with polydopamine (Fe_3O_4@PDA) composite, which was used for the adsorption of cadmium ions from an aqueous solution. In addition, the effects of environmental factors on the adsorption capacity were investigated. Furthermore, the adsorption kinetics, isotherm, and thermodynamics of the adsorbents were discussed. Results revealed that the adsorption of cadmium by Fe_3O_4@PDA reaches equilibrium within 120 min, and kinetic fitting data are consistent with the pseudo-second-order kinetics ($R^2 > 0.999$). The adsorption isotherm of Cd^{2+} on Fe_3O_4@PDA was in agreement with the Freundlich model, with the maximum adsorption capacity of 21.58 mg/g. The thermodynamic parameters revealed that adsorption is inherently endothermic and spontaneous. Results obtained from the adsorption–desorption cycles revealed that Fe_3O_4@PDA exhibits ultra-high adsorption stability and reusability. Furthermore, the adsorbents were easily separated from water under an enhanced external magnetic field after adsorption due to the introduction of an iron-based core. Hence, this study demonstrates a promising magnetic nano-adsorbent for the effective removal of cadmium from cadmium-containing wastewater.

Keywords: Magnetic nanomaterials, Dopamine modification, Adsorption, Cadmium

Introduction

Pollution by Cd(II) metals has become one of the serious environmental problems. A majority of the cadmium pollution originates from the smelting of non-ferrous metals, sintering of ores, discharge of wastewater from the electroplating industry, and preparation of phosphate fertilizers from phosphate rock [1–4]. With a long half-life, cadmium is slowly metabolized in the human body; hence, it can be easily accumulated in organs such as the kidneys of the human body [5]. The long-term exposure of humans or animals to low cadmium concentrations can lead to health issues, including kidney dysfunction and reproductive organ and bone damage, as well as malformation of the development of offspring [6]. Hence, Cd(II) is designated as a carcinogen by the World Health Organization, the International Agency for Research on Cancer, and the National Toxicology Program (USA) [7–9]. Therefore, an effective removal method of cadmium ions for the purpose of reducing environmental pollution and damage to humans and animals is an interesting topic for environmental governance.

Currently, cadmium can be removed by chemical precipitation, ion exchange, adsorption, solvent extraction, and membrane separation [10–14]. In particular, adsorption has been widely employed due to its simple operation, high efficiency, and cost-effectiveness [15]. In the past two decades, various adsorbent materials have been developed and utilized, including natural soil materials, inorganic minerals, activated carbon, zeolites, silica gel, chitosan, and polymer materials [16–22]. Compared

* Correspondence: lihongtang@ynu.edu.cn; wangshixiong@ynu.edu.cn
Key Laboratory of Medicinal Chemistry for Natural Resource (Yunnan University), Ministry of Education, School of Chemical Science and Technology, Yunnan University, No. 2, Cuihu North Road, Kunming 650091, China

to these adsorbents, magnetic nano-adsorbents can be developed and used for treating industrial wastewater due to their high specific surface area, good biocompatibility, cost-effectiveness, and rapid separation and recovery under an external magnetic field [23]. However, the superparamagnetism and high surface energy of magnetic Fe_3O_4 lead to facile agglomeration or corrosion and poor stability [24, 25]. Hence, Fe_3O_4 needs to be functionalized for the improvement of its dispersibility, stability, and contaminant removal rate. Currently, the main surface modifiers of magnetic nanoparticles include organic small molecules, high molecular-weight polymers, inorganic materials, and metal–organic frameworks [26–29].

In the past decade, dopamine (DA) has been reported to form a stable polydopamine (PDA) film with controlled thickness by self-polymerization under weakly alkaline conditions. Studies have revealed that PDA is a highly adhesive biopolymer with functional groups such as catechol, amine, and imine, which can adhere to the surface of organic or inorganic materials via the formation of covalent and non-covalent interactions (e.g., chelation, hydrogen bonds, van der Waals forces, and π–π stacking) [30, 31]. In addition, these interactions between PDA and the carrier exist between PDA and water pollutants, thereby providing a method for removing water-containing contaminants. Farnad et al. [32] have synthesized PDA nanoparticles with an average diameter of 75 nm that can efficiently adsorb Cu^{2+} from wastewater. The maximum adsorption capacity of 34.4 mg/g is obtained after the reaction is conducted for 270 min at pH 5. Zhang et al. [33] have obtained PDA-modified magnetic nanoparticles (Fe_3O_4/PDA) and subsequently used them for the removal of methylene blue, lemon yellow, Cu^{2+}, Ag^{+}, and Hg^{2+} from sewage. At an optimum pH, the maximum adsorption capacities of Fe_3O_4/PDA for these contaminants are 204.1, 100.0, 112.9, 259.1, and 467.3 mg/g, respectively. This study demonstrated the immense potential of Fe_3O_4/PDA for the removal of multiple pollutants. Huang et al. [34] have prepared a PDA-coated clay (D-clay/Fe^{3+}) with a three-dimensional network structure by using Fe^{3+} for coordination with PDA. As-prepared material exhibits good elastic response and self-repairing ability. Rhodamine 6G (Rh6G) can be removed from water through the π–π stacking interactions of the aromatic moiety between PDA and Rh6G. Gao et al. [35] have prepared a PDA-modified graphene hydrogel (PDA-GH) by a one-step approach. This material exhibits high adsorption capacities for Pb^{2+}, Cd^{2+}, rhodamine B, and p-nitrophenol. This material is also easily regenerated using low-cost desorbents such as acids and alcohols. Hence, according to previous studies, PDA exhibits a good adsorption capacity for various pollutants (i.e., heavy metals and organic pollutants), and it demonstrates broad application prospects for wastewater treatment.

Herein, Fe_3O_4 was synthesized by a solvothermal method and coated with PDA as the modifier. The amino and phenolic hydroxyl groups on PDA were utilized for the adsorption of cadmium ions, which aimed at exploring the feasibility of using Fe_3O_4 modified with polydopamine (Fe_3O_4@PDA) as the adsorbent to remove cadmium ions for wastewater treatment. In addition, the effects of various environmental parameters on the adsorption performance of Cd^{2+} on Fe_3O_4@PDA microspheres were systematically investigated by batch adsorption experiments. Furthermore, the kinetics, adsorption isotherms, thermodynamics, reusability, and stability of Fe_3O_4@PDA were evaluated. As-synthesized Fe_3O_4@PDA exhibited advantages of good stability, low biological toxicity, mild synthesis conditions, facile separation and recovery, environmental friendliness, and lack of secondary pollution. Scheme 1 shows the synthesis and structure of Fe_3O_4@PDA.

Methods

Materials

Sodium acetate anhydrous, ethylene glycol, and nitric acid (65–68 wt%) were purchased from Guangdong Chemical Reagent Engineering-Technological Research and Development Center (Guangdong, China). Trisodium citrate dihydrate and hydrochloric acid (36–38 wt%) were purchased from Tianjin Fengchuan Chemical Reagent Technologies Co., Ltd. (Tianjin, China). Sodium hydroxide, ferric chloride hexahydrate, and cadmium chloride hydrate (99%) were obtained from Guangfu Technology Development Co., Ltd. (Tianjin, China). Tris (hydroxymethyl) aminomethane and 3-hydroxytyramine hydrochloride were purchased from Aikeda Chemical Reagent Co., Ltd. (Chengdu, China). All chemicals were of analytical grade or better, and they were used without further purification. Ultrapure water was used throughout the experimental process.

Synthesis of Fe_3O_4 Microspheres

Fe_3O_4 magnetic nanoparticles were prepared by a solvothermal reaction. Briefly, $FeCl_3{\cdot}6H_2O$ (8.1 g), $Na_3C_6H_5O_7{\cdot}2H_2O$ (6 g), and CH_3COONa (21.6 g) were first dissolved in ethylene glycol (240 mL) with magnetic stirring. Second, after vigorous magnetic stirring for 30 min, the homogeneous orange-red solution was divided into three parts (80 mL/part) and transferred into three Teflon-lined stainless-steel autoclaves (100 mL) and sealed for heating at 200 °C. After reaction for 8 h, the autoclave was cooled to room temperature. The obtained Fe_3O_4 particles were collected using an external magnet and washed several times with ethanol and H_2O. Finally, the products were stored in an appropriate amount of ethanol for further use.

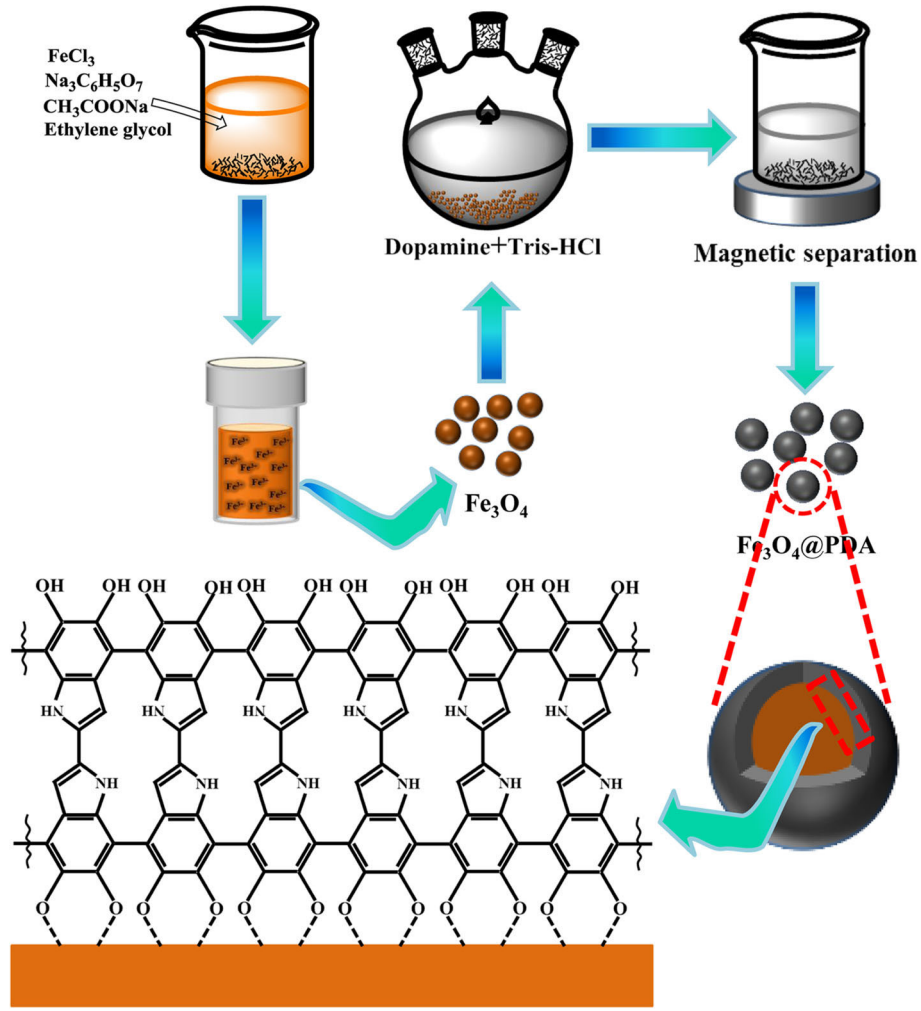

Scheme 1 Synthesis and structure of Fe_3O_4@PDA

Synthesis of Fe_3O_4@PDA Particles with Core–Shell Nanostructures

PDA-coated Fe_3O_4 nanoparticles were obtained by the polymerization of DA in an alkaline buffer at 25 °C. Briefly, the synthesized Fe_3O_4 particles were added into a 1000-mL three-necked flask containing 200 mL of Tris-HCl buffer (10 mM, pH 8.5) and subjected to sonication for 5 min. Then, 2 g of dopamine hydrochloride was weighed and dispersed in a 500-mL beaker containing 400 mL of Tris-HCl buffer (10 mM, pH 8.5) and subjected to sonication for 1 min. Then, it was added into the three-necked flask and mechanically stirred for 24 h. The synthesized Fe_3O_4@PDA particles were separated and collected using a magnet and washed several times with deionized water and ethanol, followed by drying under vacuum at 50 °C for 4 h.

Characterization

X-ray diffraction (XRD) was employed to identify the crystalline structure and phase composition of the synthesized samples in the 2θ range from 10 to 90° using Co Kα radiation. The morphology and dimensions of the samples were observed by transmission electron microscopy (TEM). Fourier transform infrared (FTIR) spectra of the samples were recorded in the wavenumber range of 400–4000 cm^{-1}. The chemical states of the samples were examined by X-ray photoelectron spectroscopy (XPS). The specific surface area was measured by N_2 adsorption using the Brunauer–Emmett–Teller (BET) method. The magnetization curve was measured at room temperature under a varying magnetic field from − 20,000 to 20,000 Oe using an MPMS-3 vibrating sample magnetometer (VSM).

Batch Adsorption Studies

Adsorption properties of the two adsorbents (i.e., Fe_3O_4 and Fe_3O_4@PDA, respectively) for the cadmium ions from an aqueous solution under various operating conditions were investigated. Adsorption experiments

were carried out in an Erlenmeyer flask with 20.0 mg of the adsorbent and 50 mL of a 20 mg/L Cd^{2+} solution (pH 7). The Erlenmeyer flask was placed in a constant-temperature shaker and subjected to shaking at 250 rpm for 120 min at 25 °C. After attaining equilibrium, the magnetic nano-adsorbent was separated from the Cd^{2+} solution by using an external magnetic field. Then, the supernatant was removed, and the concentration of cadmium ions in the initial and adsorbed solutions was estimated by atomic absorption spectrometry.

To investigate the effect of the reaction time, the reaction time was set between 15 and 2160 min. The effect of the initial cadmium solution concentration on the adsorption capacity of the adsorbent was investigated by the variation in the initial Cd^{2+} concentration between 3 and 30 mg/L. In addition, the effect of the adsorbent dose was investigated by the variation in the adsorbent dose (10–50 mg). The effect of pH on adsorption was investigated by the addition of 0.1 M NaOH or 0.1 M HCl to adjust the solution pH in the range of 4.0–9.0. Experiments were carried out at 20–45 °C to examine the effect of temperature on the adsorption performance.

The adsorption capacity for cadmium was calculated as follows:

$$q_e = (C_0 - C_e)\frac{V}{M} \quad (1)$$

where C_0 (mg/L) is the initial metal ion concentration, C_e (mg/L) is the equilibrium solution concentration, V (L) is the total solution volume, and M (g) is the mass of magnetic nanoparticles.

Reusability and Stability Studies

The reusability and stability of the adsorbent were investigated by performing 10 adsorption–desorption cycles using the Fe_3O_4@PDA adsorbent. The adsorption capacity of the adsorbent for Cd^{2+} in each cycle was analyzed. Experimental conditions for the adsorption reaction were as follows: 20 mg Fe_3O_4@PDA, 50 mL of a 20 mg/L $CdCl_2$ solution (pH 7), and reaction at 250 rpm for 120 min at 25 °C. Desorption was carried out using 50 mL of 0.5 M HCl as the desorbent, and the reaction was carried out at 250 rpm for 60 min at 25 °C. The adsorbent was separated by using a magnet after desorption and washed with deionized water and ethanol until neutral pH was achieved. After drying the adsorbents at 60 °C for 30 min, the next adsorption–desorption experiment was carried out.

Results and Discussion

Characterization of the Magnetic Adsorbents

Figure 1a shows the XRD patterns of the adsorbents. The observed diffraction peaks of Fe_3O_4 (Fig. 1a—(b)) were consistent with the standard face-centered cubic (fcc) Fe_3O_4 (JCPDS card number 19-629) (Fig. 1a—(a)) [36], and impurity peaks were not observed. Relatively strong diffraction peaks were observed at 2θ values of 18°, 30°, 35.4°, 43°, 53°, 56°, 62°, and 73°, corresponding to the standard diffraction peaks of the (111), (220), (311), (400), (422), (511), (440), and (533) crystallographic planes of Fe_3O_4, respectively, indicating that the synthesized magnetic nanoparticles are Fe_3O_4 and not other ferrites. The Fe_3O_4 particles synthesized herein exhibited cluster-like nanostructures, comprising several secondary Fe_3O_4 nanoparticles. The average size of the secondary nanocrystals at the (311) crystal plane

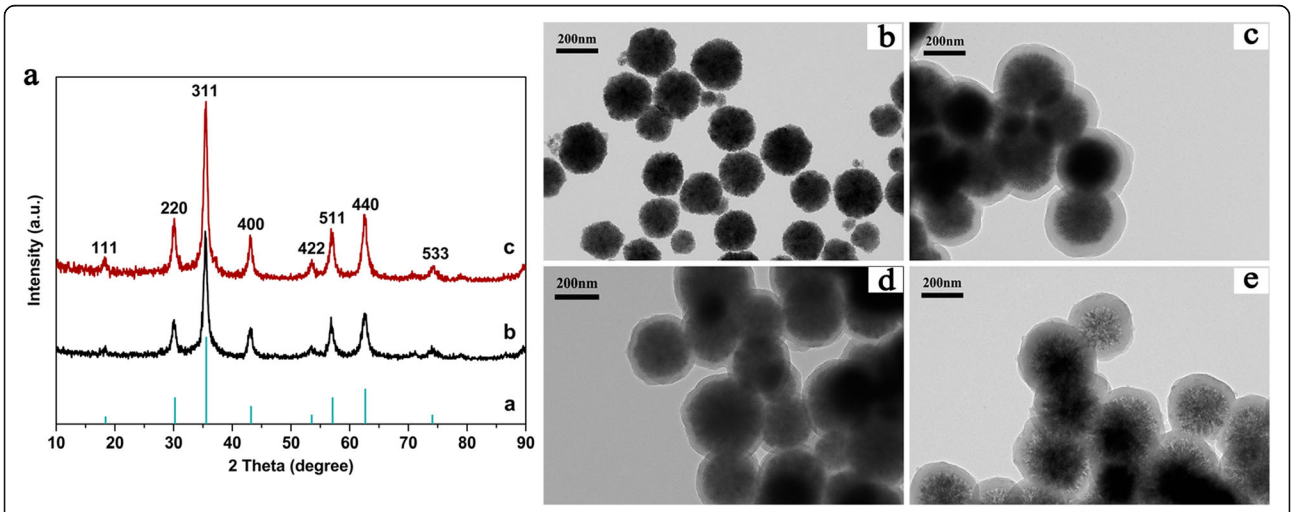

Fig. 1 **a** X-ray diffraction (XRD) patterns of (a) standard Fe_3O_4, (b) synthesized Fe_3O_4, and (c) Fe_3O_4@PDA; TEM images of **b** Fe_3O_4, **c** Fe_3O_4@PDA, **d** Fe_3O_4@PDA-Cd^{2+}, and **e** Fe_3O_4@PDA of the 10th adsorption–desorption cycles

observed in the XRD patterns was estimated to be ~ 16 nm by the Debye–Scherrer equation [37]. In the XRD pattern of Fe_3O_4@PDA particles (Fig. 1a—(c)), the main peaks were similar to those observed for original Fe_3O_4, and as the PDA shell was amorphous, diffraction peaks corresponding to PDA were not observed. The result revealed that the Fe_3O_4 crystal structure is well retained after coating with PDA. Extremely sharp diffraction peaks corresponding to Fe_3O_4 and Fe_3O_4@PDA were observed, indicative of the better crystallinity for as-prepared Fe_3O_4 [38].

Furthermore, TEM images were recorded to observe the morphology of the adsorbent and to confirm the polymerization of DA on the Fe_3O_4 core. Figure 1b shows the TEM image of bare Fe_3O_4 particles. As can be clearly observed in the TEM image, as-synthesized Fe_3O_4 exhibited a cluster of nanospheres comprising several secondary Fe_3O_4 nanoparticles. With the addition of sodium citrate as the stabilizer during the synthesis, the as-obtained Fe_3O_4 particles exhibited a uniform size (average particle diameter of 250–300 nm) and good dispersibility without agglomeration. The Fe_3O_4@PDA composites exhibited a core–shell structure (Fig. 1c). As the core, dark Fe_3O_4 particles were uniformly coated by light-colored PDA, with a 40–50-nm-thick PDA layer. Furthermore, the Fe_3O_4@PDA nanoparticles tended to agglomerate, likely related to the magnetic attraction [25] and hydrogen bonding between the Fe_3O_4@PDA particles. In addition, owing to the high surface energy of the nanoparticles, the system automatically changed in the direction of the decreased surface area, leading to the nanoparticle agglomeration [39]. Figure 1d shows the Fe_3O_4@PDA particles after the adsorption of cadmium ions. The PDA coating was darker in color, and the core structure was unchanged. Moreover, the dispersibility of Fe_3O_4@PDA-Cd^{2+} was better than that of Fe_3O_4@PDA particles due to the decrease in the surface energy of Fe_3O_4@PDA after the adsorption of Cd^{2+}. By the comparison of Fig. 1d and e, after 10 adsorption–desorption cycles, the PDA coating remained intact, but the Fe_3O_4 core density decreased because the desorbent (0.5 mol/L HCl) corroded a part of the secondary Fe_3O_4 nanoparticles. Although the core was corroded, the Fe_3O_4@PDA structure was retained after 10 adsorption–desorption cycles, indicating that PDA exhibits a good protective effect on the exposed Fe_3O_4 particles.

The BET specific surface areas of Fe_3O_4 and Fe_3O_4@PDA were estimated to be 61.84 m^2/g and 14.23 m^2/g, respectively. The decrease in the specific surface area of Fe_3O_4@PDA corresponded to the increase in the particle size of the magnetic nanoparticles after coating with DA. In addition, the agglomeration of Fe_3O_4@PDA led to the decrease in the specific surface area [40].

Figure 2a shows the FTIR spectra of Fe_3O_4, PDA, Fe_3O_4@PDA, and Fe_3O_4@PDA-Cd^{2+}. A strong absorption peak observed 599 cm^{-1} corresponded to the Fe–O–Fe bond (Fig. 2a—(a)) [41]. In this study, sodium citrate was added to improve the dispersibility of Fe_3O_4; hence, absorption peaks observed at 1628 and 1384 cm^{-1} in the FTIR spectrum of Fe_3O_4 correspond to the residual carboxylate group [42]. In addition, the bands observed at 1070 and 3430 cm^{-1} corresponded to the C–H bending vibration and stretching vibrations for surface-adsorbed O–H of water, respectively [43]. In the FTIR spectrum of PDA microspheres (Fig. 2a—(b)), the peak observed at 1620 cm^{-1} corresponded to the stretching vibration of the aromatic ring and the bending vibration of N–H [44]. The peak observed at 1510 cm^{-1} corresponded to the N–H shearing vibration of the amino group, and the peaks observed at 1384 and 1285 cm^{-1} corresponded to the bending and stretching vibrations of C–O–H, respectively, and the peak observed at 1120 cm^{-1} corresponded to the C–O stretching vibrations [45]. The peak corresponding to PDA at 3430 cm^{-1} was broader than that observed in the FTIR spectrum of Fe_3O_4, possibly related to the superposition of the stretching vibrations of the amino group, phenolic hydroxyl group, and adsorbed water in the DA polymer [40]. Absorption peak characteristics of Fe_3O_4 and PDA polymers in the FTIR spectrum of the Fe_3O_4@PDA composites were observed [Fig. 2a—(c)]. Therefore, the results obtained from FTIR spectroscopy revealed that DA is successfully coated on the Fe_3O_4 surface and that the Fe–O–Fe peak of Fe_3O_4@PDA is weaker than that of Fe_3O_4, indicating that the thicker PDA coating exhibits a certain shielding effect. In the FTIR spectrum of Fe_3O_4@PDA-Cd^{2+} (Fig. 2a—(d)), after the adsorption of heavy metal ions, Fe_3O_4@PDA exhibited a peak shift from 3 to 7 for the peaks observed at 3420, 1622, 1291, and 1123 cm^{-1}, with a slightly weakened peak intensity. All of these peaks corresponded to amino and phenolic hydroxyl groups, indicating that these two groups are the main functional groups that interact with metal ions.

To further verify the FTIR spectra, XPS profiles of Fe_3O_4@PDA before and after adsorption were recorded. The wide-scan spectrum revealed C 1s (285.90 eV), N 1s (400.28 eV), O 1s (532.72 eV), and Fe 2p (711.22 eV) peak characteristics of Fe_3O_4@PDA, and the peak intensity revealed that the surface oxygen content of Fe_3O_4@PDA is greater than that of nitrogen (Fig. 2b). The Cd 3d peak was observed in the wide-scan spectrum of Fe_3O_4@PDA-Cd^{2+}, indicating that Cd^{2+} can be adsorbed on the Fe_3O_4@PDA surface. To verify the peaks observed in the FTIR spectra, Cd^{2+} interacted with -OH and -NH_2 on the adsorbent surface. Figure 2c and d show the comparison of the O 1s and N 1s binding energies for Fe_3O_4@PDA before and after adsorption, respectively. Binding energy peaks in the O 1s spectrum before adsorption were

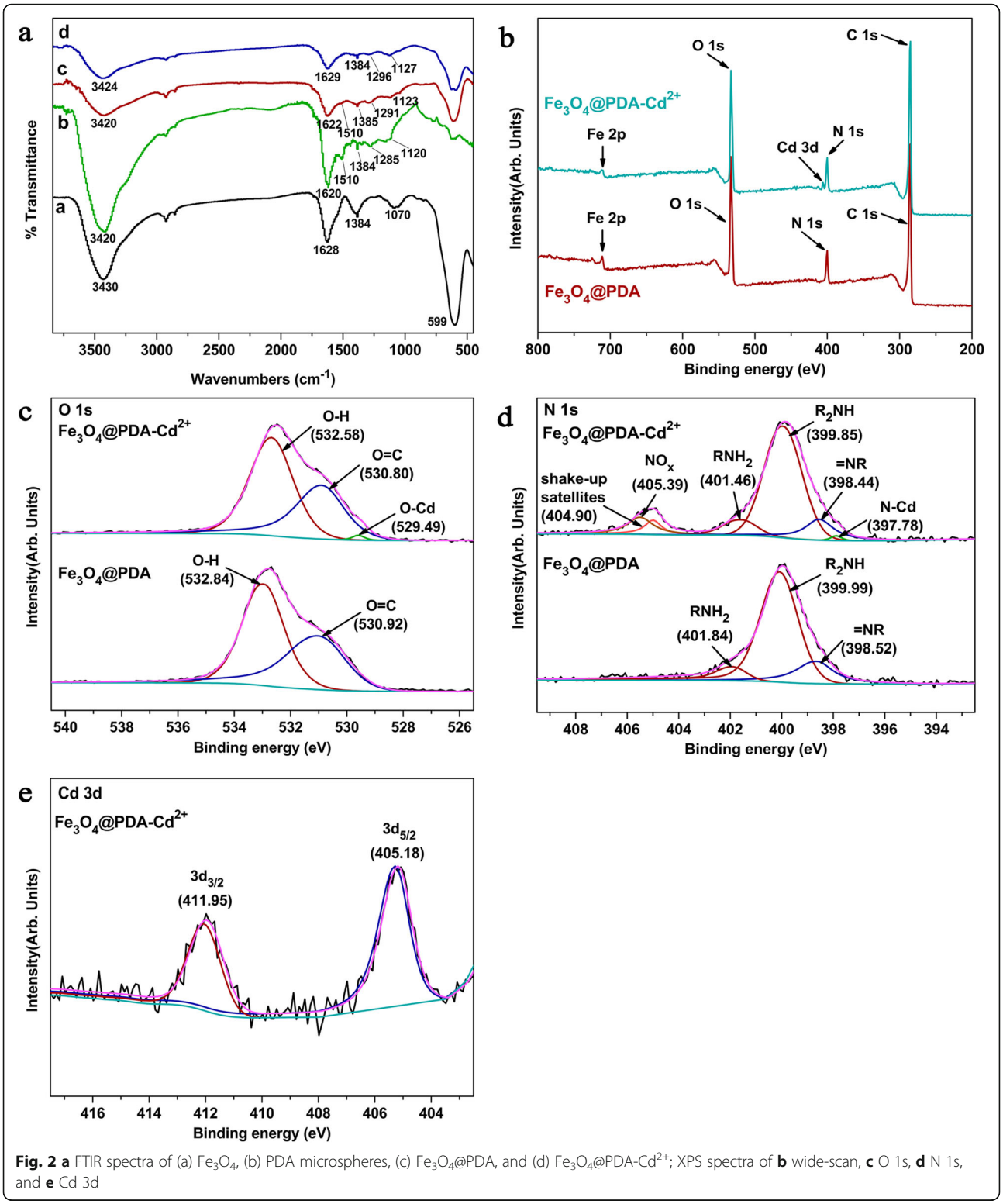

Fig. 2 **a** FTIR spectra of (a) Fe_3O_4, (b) PDA microspheres, (c) Fe_3O_4@PDA, and (d) Fe_3O_4@PDA-Cd^{2+}; XPS spectra of **b** wide-scan, **c** O 1s, **d** N 1s, and **e** Cd 3d

observed at 532.58 and 530.80 eV, corresponding to O in -OH and -C=O [46], respectively. Among these peaks, -C=O was obtained by the conversion of the phenolic hydroxyl groups into quinone (Scheme 2). By the comparison of the peak areas of -OH and -C=O, the -OH content on the adsorbent surface is known to be greater than the -C=O content. After the adsorption of cadmium, the binding energies of -OH and -C=O shifted to low

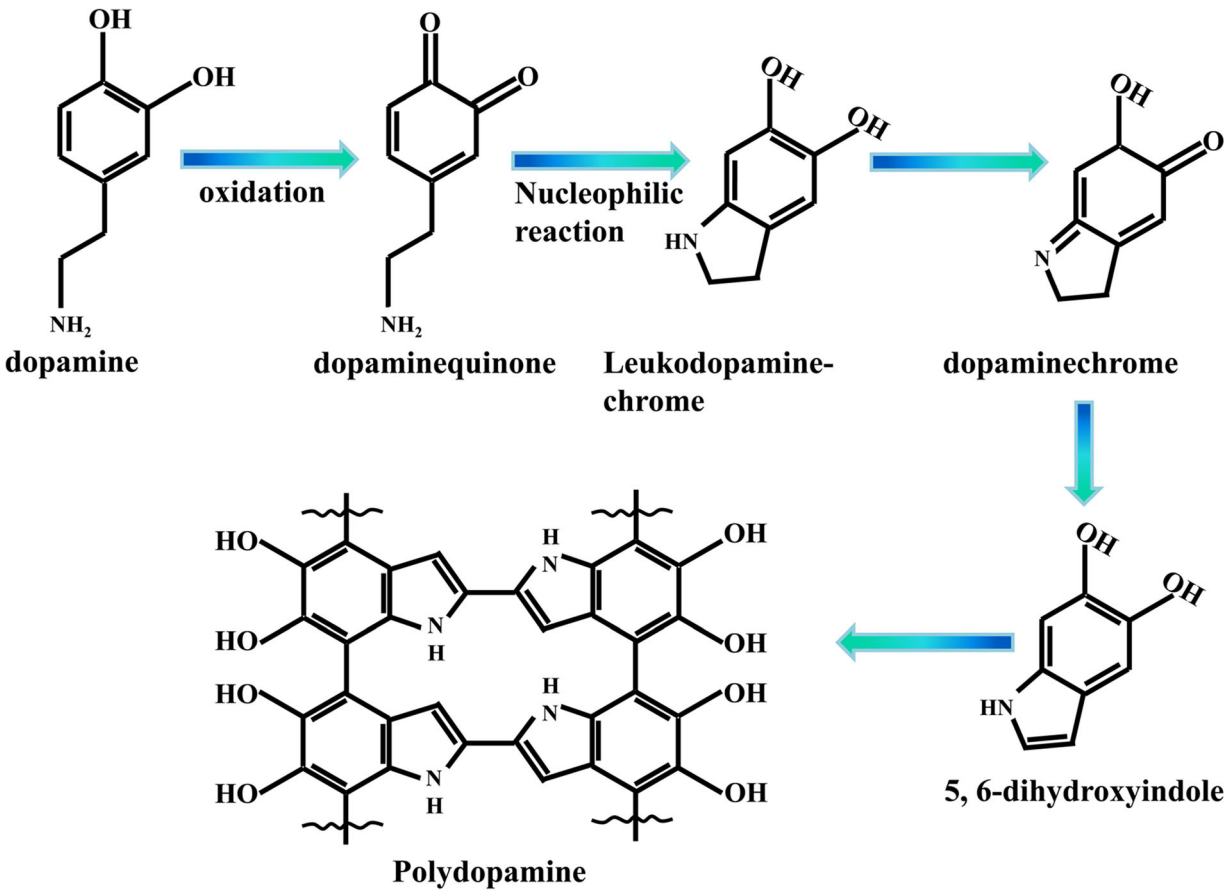

Scheme 2 Synthetic of polydopamine

binding energies due to the donation of the lone-pair electrons of O to Cd^{2+}, leading to the decrease in the electron cloud density of O [47]. The new peak observed at 529.49 eV was speculated to be related to the complexation of Cd^{2+} with O on the Fe_3O_4@PDA surface. In the N 1s spectrum before adsorption, =N–R (398.52 eV), R_2N–H (399.99 eV), and R–NH_2 (401.84 eV) were observed [48]. The three peaks observed in the adsorbed N 1s spectrum shifted toward the direction of low binding energy, corresponding to the decrease in the electron cloud density of N caused by the sharing of the lone-pair electrons of N with Cd^{2+}. Based on this result, the new peak observed at 397.78 eV was presumed to originate owing to the complexation of Cd^{2+} with N. As the purity of the used reagent ($CdCl_2$) was 99%, N-containing impurities were introduced during the adsorption; hence, peaks observed at 404.90 and 405.39 eV correspond to the shake-up satellites and nitrogen oxides, respectively [49]. The peak area and peak intensity of O–Cd and N–Cd were low, indicating that only a part of O and N on Fe_3O_4@PDA participates in the reaction. The peaks of Cd 3d (Fig. 2e) were divided into the main peak of Cd $3d_{5/2}$ (405.18 eV) and the secondary peak of Cd $3d_{3/2}$ (411.95 eV). Generally, the binding energy of Cd $3d_{5/2}$ of CdO is 404.8 eV [50]; however, the binding energy of Cd $3d_{5/2}$ in this study was 405.18 eV, indicating that Cd^{2+} interacted with not only oxygen functional groups but also nitrogen functional groups.

Hence, the O 1s, N 1s, and Cd 3d XPS spectra confirmed the results obtained from FTIR spectroscopy; Cd^{2+} is adsorbed by the action of the amino and hydroxyl groups on the Fe_3O_4@PDA surface; and the hydroxyl group plays a major role.

To investigate the magnetic properties of the materials, the VSM was utilized to measure the hysteresis curve of the materials. With the increase in the magnetic field strength, the magnetization of Fe_3O_4 and Fe_3O_4@PDA increased (Fig. 3). The saturation magnetization value of Fe_3O_4 nanoparticles was estimated to be 64.9 emu/g, while that of the Fe_3O_4@PDA composite was reduced to 48.8 emu/g. This decrease was related to the deposition of a large number of non-magnetic DA polymers on Fe_3O_4.

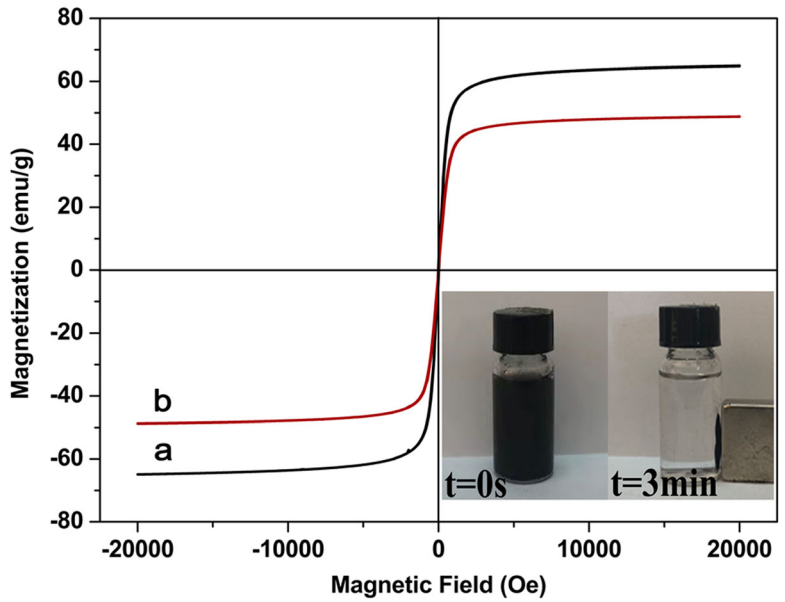

Fig. 3 Magnetization curves of **a** Fe_3O_4 and **b** Fe_3O_4@PDA nanoparticles at room temperature

Hysteresis was not observed in the hysteresis curves of Fe_3O_4 and Fe_3O_4@PDA, and the remanence and coercivity were close to zero, indicating that the materials exhibit a superparamagnetic character [33]. As can be observed in the lower right side of Fig. 3, Fe_3O_4@PDA was dispersed in water, affording a homogeneous suspension. Although the saturated magnetization value of Fe_3O_4@PDA was less than that of Fe_3O_4, Fe_3O_4@PDA was separated from wastewater by using an external magnetic field in 3 min. After removing the applied magnetic field, Fe_3O_4@PDA was rapidly dispersed into the solution, facilitating the collection, regeneration, and reuse of the adsorbents.

Adsorption of Cd^{2+} in Batch Systems

The adsorption capacity of the adsorbents for heavy metal ions is mainly affected by factors such as reaction time, heavy metal-ion concentration, adsorbent dose, pH, and reaction temperature. Hence, batch adsorption experiments are carried out on the adsorbent to examine the effect of the above factors on the reaction, as well as the kinetics, isotherm, and thermodynamic properties of the adsorbent.

Effect of Contact Time and Kinetics Study

Adsorption time is one of the important factors that affect the performance of an adsorbent. Figure 4a shows the effect of the adsorption time on adsorption capacity. From this figure, the adsorption capacity of Fe_3O_4 and Fe_3O_4@PDA for Cd^{2+} increased with time and tended to level after a certain time. Both adsorbents exhibited a more rapid adsorption rate before 90 min, and then the adsorption rates tended to be flat. Fe_3O_4 and Fe_3O_4@PDA reached the adsorption equilibrium at 240 and 120 min, respectively, because the difference in the concentration between Cd^{2+} and the solution on the adsorbent surface at the start of adsorption leads to the rapid movement of cadmium from the solution to the adsorbent surface. At the same time, a large number of adsorption active sites are present on the adsorbent surface, and Cd^{2+} in the aqueous solution exhibits a greater chance of occupying these sites. With the increase in the adsorption time, the active sites were predominantly occupied, and the positive charge on the adsorbed metal ions also repelled the metal ions in the water, increasing the difficulty in the adsorption of Cd^{2+} by the adsorbents. Hence, the adsorption rate gradually decreases and eventually reaches equilibrium. As Fe_3O_4@PDA comprises polar groups such as amino and hydroxyl groups, the affinity for water is greater than that for Fe_3O_4, which is beneficial for the contact of cadmium ions on the adsorbent surface; therefore, the equilibrium time of Fe_3O_4@PDA is shorter.

To analyze the adsorption kinetics of Fe_3O_4@PDA, adsorption data were simulated by the pseudo-first-order and pseudo-second-order kinetics models, which were expressed in Eqs. (2) and (3), respectively [51, 52].

$$\ln(q_e - q_t) = \ln q_e - k_1 t \tag{2}$$

$$\frac{t}{q_t} = \frac{1}{k_2 q_e^2} + \frac{t}{q_e} \tag{3}$$

where k_1 (min^{-1}) is the pseudo-first-order rate constant, k_2 ($g \cdot mg^{-1} \cdot min^{-1}$) is the pseudo-second-order rate constant, and q_e and q_t represent the loading of Cd^{2+} at equilibrium and at time t, respectively.

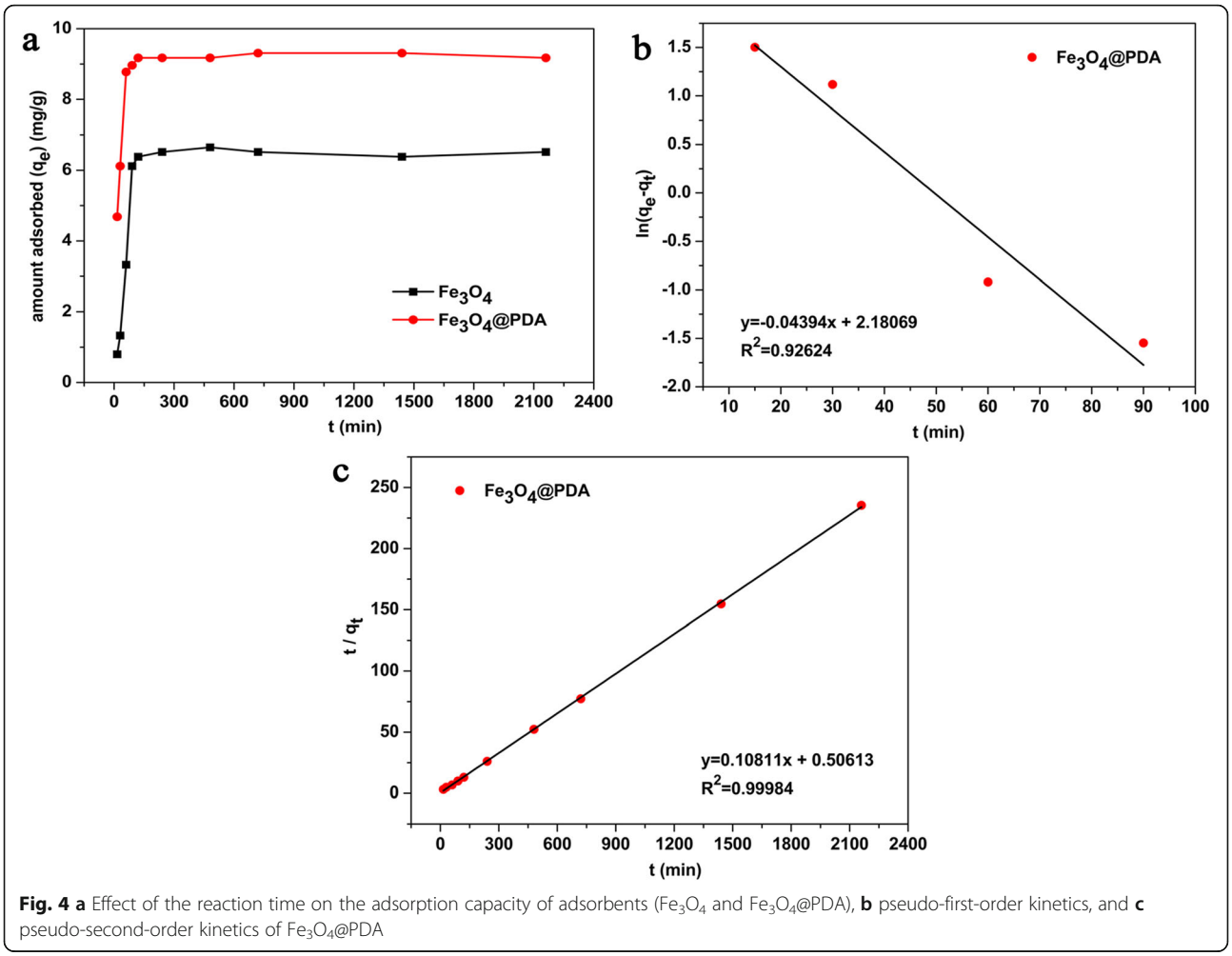

Fig. 4 **a** Effect of the reaction time on the adsorption capacity of adsorbents (Fe_3O_4 and Fe_3O_4@PDA), **b** pseudo-first-order kinetics, and **c** pseudo-second-order kinetics of Fe_3O_4@PDA

A linear relationship between $\ln(q_e - q_t)$ and t at different initial cadmium concentrations was observed (Fig. 4b). Figure 4c shows a graph obtained by the further analysis of q_t versus t using the pseudo-second-order rate law. The parameter values for the pseudo-first-order and pseudo-second-order kinetics were determined by the slope and intercept of the corresponding curve, respectively. Table 1 summarizes the results obtained. The correlation coefficient for the pseudo-second-order kinetics model (R^2 = 0.9998) was greater than that of the pseudo-first-order kinetics model (R^2 = 0.9262). Compared with q_e ^{cal} (8.852 mg/g) observed for the pseudo-first-order kinetics, q_e ^{cal} (9.250 mg/g) for the pseudo-second-order kinetics model was similar to the experimental value of q_e (9.176 mg/g). Therefore, the adsorption kinetics of Fe_3O_4@PDA follows the pseudo-second-order model, indicating that the adsorption of Cd^{2+} by Fe_3O_4@PDA is possibly consistent with chemical adsorption; that is, electrons are shared or exchanged between the adsorbent and adsorbate, and Cd^{2+} is adsorbed by the formation of covalent bonds or ion exchange [53].

Effect of Concentration and Adsorption Isotherms

The adsorption performance of the adsorbents (i.e., Fe_3O_4 and Fe_3O_4@PDA) was determined at Cd^{2+} concentrations ranging from 3 to 30 mg/L. Figure 5a shows the experimental result obtained. With the increase in the Cd^{2+} concentration, the q_e of the adsorbents increased because increased amounts of Cd^{2+} were available at high concentrations, increasing the possibility of contact between Cd^{2+} and the adsorbent active sites, and high concentration of cadmium also provided a higher driving force for the ions from the solution to the adsorbent surface. In addition, the adsorption capacity of Fe_3O_4@PDA was greater than that of Fe_3O_4 under the same adsorption conditions, indicating that the surface-dopamine-modified magnetic nanoparticles are more favorable for removing cadmium ions.

To understand the mechanism via which cadmium was adsorbed on Fe_3O_4@PDA, three isotherm adsorption models (i.e., Langmuir, Freundlich, and Dubinin–Radushkevich, respectively) were employed in this study

Table 1 Kinetics adsorption parameters of Cd^{2+} by Fe_3O_4@PDA

q_e ^{exp} (mg/g)	Pseudo-first-order			Pseudo-second-order		
	K_1 (min^{-1})	q_e ^{cal} (mg/g)	R^2	K_2 ($g \cdot mg^{-1} \cdot min^{-1}$)	q_e ^{cal} (mg/g)	R^2
9.176	0.04394	8.852	0.9262	0.02309	9.250	0.9998

to describe the adsorption equilibrium of Fe_3O_4@PDA. These isotherm equations were expressed as follows:

$$\frac{C_e}{q_e} = \frac{1}{bq_m} + \frac{C_e}{q_m} \quad (4)$$

$$\log q_e = \log k + \frac{1}{n} \log C_e \quad (5)$$

$$\ln q_e = \ln q_d - K_d \varepsilon^2 \quad (6)$$

where q_e (mg/g) and C_e (mg/L) are the adsorption capacity and Cd^{2+} concentration at equilibrium, respectively; b (L/mg) is the Langmuir adsorption equilibrium constant; and q_m (mg/g) is the maximum adsorption capacity. The K [(mol/g)/(mol/L)$^{1/n}$] value can be regarded as the adsorption amount with Cd^{2+} as the unit concentration and $1/n$ as the indicator of the adsorption strength. q_d (mol/g) is the maximum adsorption capacity, K_d (mol^2/kJ^2) is a constant related to adsorption energy, and ε is the Polanyi potential ($\varepsilon = RT \ln(1 + 1/C_e)$, where the unit of C_e is mol/L).

In addition, the equilibrium parameter R_L [$1/(1 + bC_o)$], highest initial solute concentration in the concentration gradient C_0 (mg/L)), and the mean free energy of adsorption, E_d [$(2K_d)^{-1/2}$, kJ/mol] were estimated. R_L was utilized

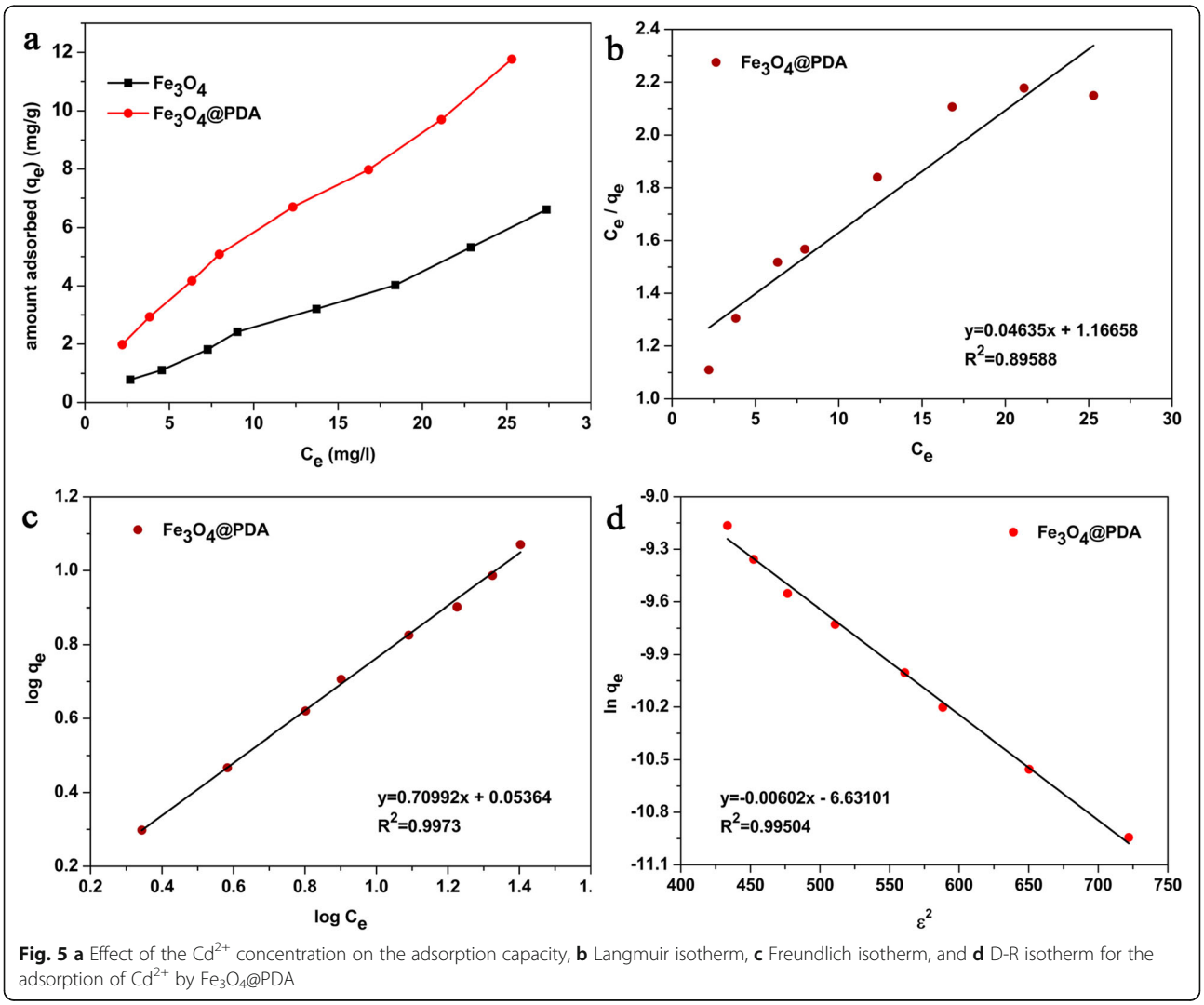

Fig. 5 **a** Effect of the Cd^{2+} concentration on the adsorption capacity, **b** Langmuir isotherm, **c** Freundlich isotherm, and **d** D-R isotherm for the adsorption of Cd^{2+} by Fe_3O_4@PDA

to determine whether the adsorption process is favorable. E_d can be used to determine the type of adsorption. E_d values of 1–8 kJ/mol were indicative of physical adsorption (such as van der Waals forces), while those of 8–16 kJ/mol were indicative of ion exchange. An E_d value of between 20 and 40 kJ/mol revealed that the adsorption reaction is chemisorption [54].

The isothermal curves constructed with the Langmuir, Freundlich, and D-R models correspond to b, c, and d in Fig. 5, respectively. Table 2 summarizes the calculated isothermal parameters. The correlation coefficient from the fitting of the curve revealed that the Freundlich model ($R^2 = 0.9973$) is more suitable than the Langmuir model ($R^2 = 0.8959$) and D-R model ($R^2 = 0.9950$) for describing the adsorption of Cd^{2+} by Fe_3O_4@PDA. Hence, the adsorption of Cd^{2+} can be described by the Freundlich isotherm, indicating that Cd^{2+} is adsorbed on an uneven surface by the multilayer and that the energy distribution for the surface-active sites of the adsorbent is uneven [55]. Simultaneously, $n > 1$ reflects the high affinity between the adsorbate and adsorbent; hence, adsorption is favorable [56, 57]. The maximum adsorption capacity (q_m) obtained by the Langmuir model was 21.58 mg/g. The R_L value was between 0 and 1, indicative of the advantageous reaction of Fe_3O_4@PDA to adsorb Cd^{2+} [58]. In addition, in this study, the E_d value was calculated to be 9.114 kJ/mol, which was within the range of values reflecting the ion exchange mechanism (8–16 kJ/mol) and was similar to that reflecting the electrostatic adsorption (1–8 kJ/mol). Hence, by the combination of the E_d value and the preceding analysis for pseudo-second-order kinetics, the adsorption of Cd^{2+} on Fe_3O_4@PDA is predominated by ion exchange and electrostatic adsorption mechanisms.

The q_m value of Fe_3O_4@PDA was compared with the adsorption capacity of Cd^{2+} for other previously reported adsorbents (Table 3). The q_m value widely varied for different adsorbents. Generally, commercial exchange resins and activated carbons exhibit higher adsorption capacities due to their higher specific surface areas, but the recovery and separation of these resins and carbons are not possible. The q_m value of Fe_3O_4@PDA adsorbing Cd^{2+} was relatively reasonable (Table 3), and Fe_3O_4@PDA could be recovered by a magnetic field, indicating that the adsorbent can be possibly applied for the removal of Cd^{2+} from wastewater.

Effect of Temperature and Thermodynamic Parameters

Temperature is crucial for adsorption. Therefore, the effect of temperatures in the range of 293.15–318.15 K on the adsorption performance of Fe_3O_4@PDA is examined. With increasing temperature, the adsorption capacity of the adsorbents for Cd^{2+} increased (Fig. 6a). This trend indicated that the adsorption of Cd^{2+} by Fe_3O_4@PDA is an endothermic process, and high temperature is favorable for the adsorption of Cd^{2+}. In addition, high temperature promotes the mobility of metal ions, thereby increasing the possibility of contact between Cd^{2+} and active sites as well as the adsorption capacity of the adsorbents.

At the same time, various thermodynamic parameters were calculated to examine the thermodynamics properties of Fe_3O_4@PDA, such as entropy (ΔS^o), enthalpy (ΔH^o), and Gibbs free energy (ΔG^o). The calculated equations were expressed as follows:

$$K_e = \frac{q_e}{c_e} \tag{7}$$

$$\Delta G^o = -RT \ln K_e \tag{8}$$

$$\Delta G^o = \Delta H^o - T\Delta S^o \tag{9}$$

The van 't Hoff equation can be derived from Eqs. (8) and (9) as follows:

$$\ln K_e = -\frac{\Delta H^o}{RT} + \frac{\Delta S^o}{R} \tag{10}$$

where q_e (mg/g) is the adsorption capacity of the adsorbent for cadmium ions at the reaction equilibrium, C_e (mg/L) is the concentration of cadmium ions in the solution at equilibrium, K_e (mL/g) is the thermodynamic equilibrium constant (the value depends on the temperature), T (K) is the absolute temperature, and R [8.314 J/(mol·K)] is the gas constant.

Figure 6b shows the relationship between $\ln K_e$ and $1/T$ of Cd^{2+} adsorbed by Fe_3O_4@PDA. After fitting, the straight line with a linear correlation coefficient R^2 of 0.9636 was obtained. The R^2 value revealed that $\ln K_e$ exhibits a basic linear relationship with $1/T$. The thermodynamic parameters were calculated from the slope and intercept of the curve. Table 4 summarizes the results obtained. With increasing temperature, the ΔG° of cadmium ions decreased from − 13.196 to − 16.638 kJ/mol (Table 4), indicating that the adsorption of Cd^{2+} by Fe_3O_4@PDA is a spontaneous reaction and that the degree of a spontaneous reaction increases with temperature. The increase of K_e with temperature and $\Delta H^\circ > 0$ revealed that the adsorption is an endothermic reaction as Cd^{2+} is solvated in water to form

Table 2 The Langmuir, Freundlich, and D-R isotherm parameters for the adsorption of Cd^{2+} by Fe_3O_4@PDA

Langmuir model				Freundlich model			D-R model			
b (L/mg)	q_m (mg/g)	R_L	R^2	K (mg/g)	n	R^2	q_d (mol/g)	K_d (mol^2/kJ^2)	E_d (kJ/mol)	R^2
0.03973	21.58	0.4562	0.8959	1.132	1.409	0.9973	1.319×10^{-3}	6.02×10^{-3}	9.114	0.9950

Table 3 Comparison of the maximum adsorption capacities of Fe_3O_4@PDA with some adsorbents cited in the literature

Adsorbents		q_m (mg/g)	pH	$C_{0\ (Cd)}$ (mg/L)	References
Nano-hydroxyapatite nanorods		92	5.8	100–500	[1]
Nano-hydroxyapatite chitosan composites		122			
Fe_3O_4@SiO_2@m-SiO_2–NH_2		884.906	6	20–843	[20]
Fly ash/chitosan (A-FA/Ch) composite		87.72	8	25–600	[21]
Surface-modified Eucalyptus seeds by sulfuric acid (SMES-S)		71.15	5	20–100	[52]
Surface-modified Eucalyptus seeds by hydrochloric acid (SMES-H)		64.16			
Nano zero-valent iron particles		769.2	–	25–450	[57]
Biopolymeric sorbent: sporopollenin		2.23	7	0–250	[59]
Poly (sodium acrylate)–graphene oxide		225.7	6	20–600	[60]
Zero-valent iron-coated biochars (magnetic ones)	MBC_1	38.00	5	50–600	[61]
	MBC_2	41.25			
Multiwalled carbon nanotubes (MWCNTs)	Raw-MWCNT	1.260 ± 0.02	8	0.1–5	[62]
	O-MWCNT	22.39 ± 0.36			
	E-MWCNT	21.67 ± 0.40			
Sawdust of *Pinus sylvestris*		15.27	4	1–50	[63]
		19.08	5		
		6.72	7		
Mustard husk		42.85	6	1–5	[64]
Mercaptoacetic-acid-modified orange peel (MOP)		136.05	7	50–1000	[65]
Polydopamine-modified Fe_3O_4		21.58	7	3–30	This study

hydrated ions. For the adsorption of the ions, dehydration is required to some extent. Hence, it is crucial to absorb heat, which is provided by temperature. The higher the temperature, the higher the degree of dehydration for hydrated ions, which is also one of the reasons for the favorable adsorption at high temperatures [59]. The $\Delta H°$ value can be used to determine whether adsorption is physical or chemical adsorption. The $\Delta H°$ value for physical adsorption is between 2 and 21 kJ/mol, while the $\Delta H°$ value for chemisorption is between 80 and 200 kJ/mol [66]. The $\Delta H°$ value calculated in this experiment was ~ 25.714 kJ/mol, suggesting that the type of adsorption is physico-

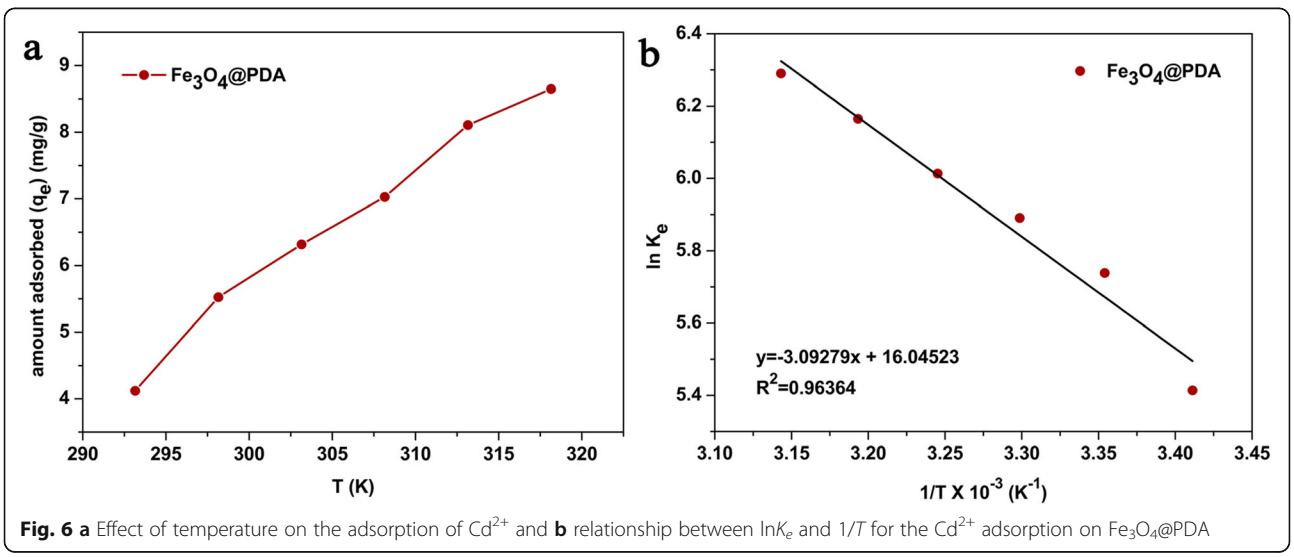

Fig. 6 a Effect of temperature on the adsorption of Cd^{2+} and **b** relationship between lnK_e and 1/T for the Cd^{2+} adsorption on Fe_3O_4@PDA

Table 4 Thermodynamic parameters for the adsorption of Cd^{2+} by Fe_3O_4@PDA

T (K)	K_e (mL/g)	$\Delta G°$ (kJ/mol)	$\Delta H°$ (kJ/mol)	$\Delta S°$ [kJ/(K·mol)]
293.15	224.55	− 13.196	25.714	0.13340
298.15	310.56	− 14.224		
303.15	361.64	− 14.847		
308.15	408.81	− 15.406		
313.15	475.81	− 16.051		
318.15	539.22	− 16.638		

chemical adsorption rather than pure physical or chemical adsorption. The entropy change $\Delta S°$ was positive [0.1334 kJ/(K·mol)], indicating that adsorption increases the chaos on the adsorbent surface and that the randomness for the adsorption of cadmium ions at the solid–solution interface increases at the active sites of the Fe_3O_4@PDA [67]. At the same time, the positive value of $\Delta S°$ also revealed that ion exchange occurs on the adsorbent surface [56].

Effect of Adsorbent Dose

Figure 7a shows the comparison of the effects of different adsorbent doses (10–50 mg) on the adsorption of cadmium ions. The course of the curve shown in Fig. 7a indicated that the adsorption capacity gradually decreases with the increase in the adsorbent dose. The increased adsorbent dose provided additional active sites, but at high adsorbent concentrations, the adsorbent underwent agglomeration, thereby decreasing the unoccupied adsorption active sites and effective surface area. In addition, if the initial concentration and volume of Cd^{2+} are constant, the number of cadmium ions contacted and adsorbed by the adsorbent per unit mass decreases with the increase in the adsorbent dose, and the active sites of the adsorbents are not saturated. Hence, with the increase in the adsorbent dose, the adsorption capacity of Cd^{2+} gradually decreases. Under the same dose of adsorbents, the adsorption capacity of Fe_3O_4@PDA for cadmium ions was greater than that of Fe_3O_4, indicating that Fe_3O_4@PDA exhibits advantages over bare Fe_3O_4 in cadmium removal.

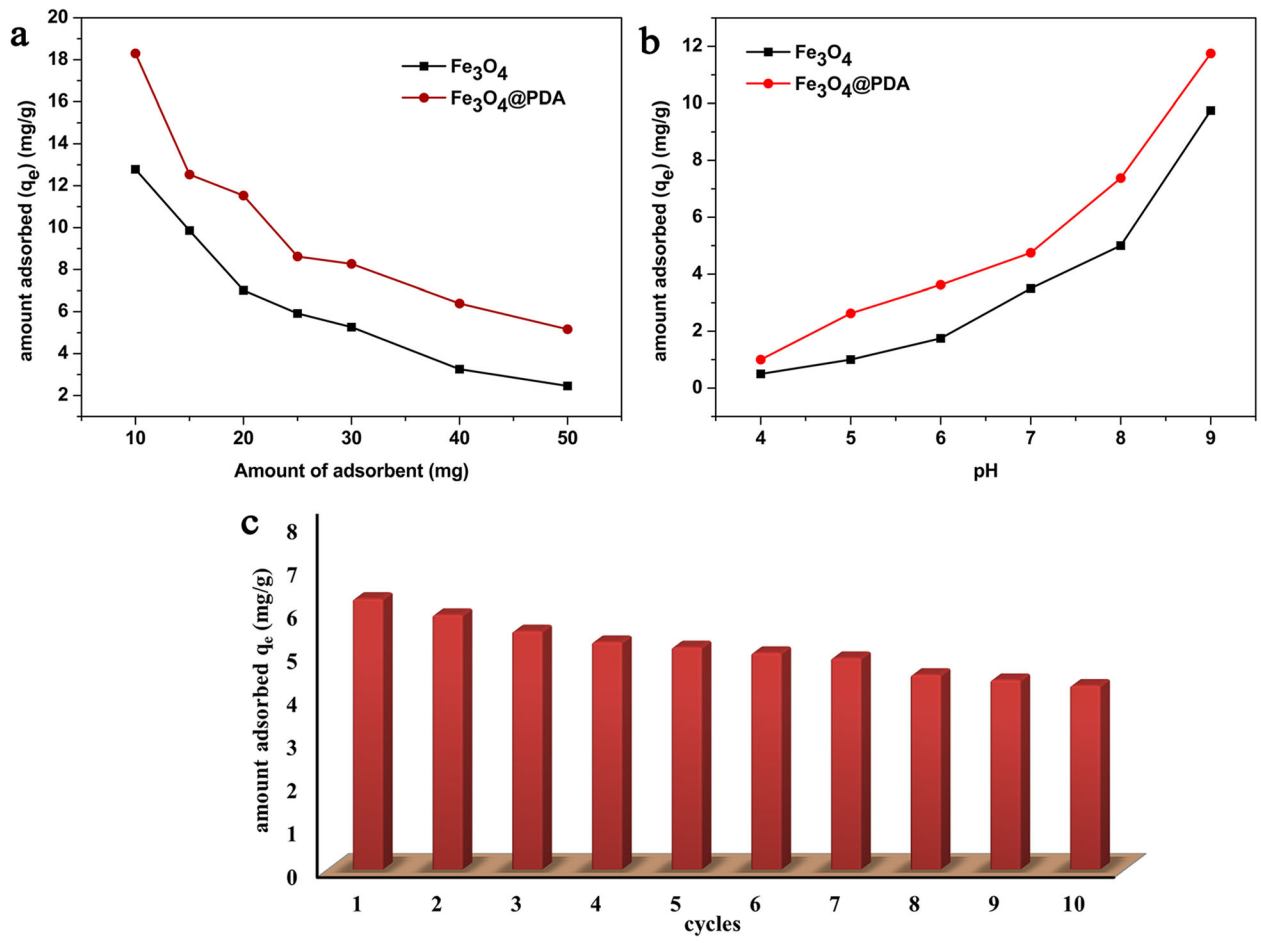

Fig. 7 **a** Effect of different adsorbent doses on the adsorption of Cd^{2+}, **b** effect of pH on the uptake of metal ions by the adsorbents, and **c** variation of the adsorption capacity of Fe_3O_4@PDA for Cd^{2+} with the number of adsorption–desorption cycles

Effect of pH

The solution pH is also one of the most important factors affecting adsorption. The adsorption of Cd^{2+} is mainly affected by the surface charges on the adsorbents, and the surface charges of the adsorbents are affected by the solution pH. Considering the degree of tolerance for adsorbents to acid and base, the chemical states of cadmium ions in an aqueous solution [i.e., Cd^{2+}, $Cd(OH)^{+}$, $Cd(OH)_2$, and $Cd(OH)_3^{-}$] [60], and the actual conditions of environmental water samples, pH values of between 4 and 9 were selected to investigate the adsorption of Cd^{2+} by the adsorbents.

Figure 7b shows the experimental results. With the increase in the solution pH, the adsorption amount of the adsorbents on Cd^{2+} significantly increased. At low solution pH, the concentration and activity of H^{+} in the solution were extremely high, which can compete with Cd^{2+} for adsorption and occupy the active site on the adsorbent surface, leading to the low adsorption capacity of Cd^{2+} by the adsorbent [61]. At low solution pH, the adsorption of cadmium must overcome the repulsive force between the positively charged Fe_3O_4@PDA surface and Cd^{2+} through chemical interactions with sufficient energy rather than through electrostatic attractions [68]. At solution pH values of between 6.0 and 8.0, the main chemical states of cadmium were Cd^{2+} (minor) and $Cd(OH)^{+}$ (major) [69]. As the affinity of $Cd(OH)^{+}$ was better than that of Cd^{2+}, it can be adsorbed on the adsorbent surface not only by electrostatic adsorption and ion exchange but also by hydrogen bonds. With the further increase in the solution pH, the protonation sites on the adsorbent surface decreased, and the negative charge increased, facilitating the adsorption of Cd^{2+} and $Cd(OH)^{+}$ on the deprotonation active sites of the adsorbent by electrostatic adsorption [70]. Hence, the increase in pH is beneficial to the adsorption of heavy metal cadmium. The precipitation of cadmium at pH 8.8 was calculated from the precipitation constant of $Cd(OH)_2$(s) ($K_{sp} = 7.2 \times 10^{-15}$) and the initial Cd^{2+} concentration (20 mg/L). Thus, at a solution pH from 8.0 to 9.0, the adsorption capacities of both adsorbents sharply increase (Fig. 7b). Moreover, the high adsorption amount at pH 9.0 resulted from the formation of a $Cd(OH)_2$ precipitate rather than the adsorption of cadmium on the adsorbent. Nevertheless, at a solution pH between 4.0 and 8.8, the adsorption capacity of Fe_3O_4@PDA was greater than that of bare Fe_3O_4, indicating that the Fe_3O_4@PDA adsorbent can be used in the wide pH range of 4.0–8.8 for treating Cd^{2+}-containing wastewater.

Combined with the kinetics, isotherm model, and thermodynamic analysis, the adsorption of cadmium by Fe_3O_4@PDA is a physico-chemical process, and the adsorption mechanism is mainly electrostatic adsorption and ion exchange, supplemented by complexation. At the same time, combined with the effect of pH on the adsorption result, the adsorption mechanism can be obtained from Eqs. 11–18 [62–64]:

$$-NH_2 + H^{+} \rightarrow -NH_3^{+} \tag{11}$$

$$-NH_2 + Cd^{2+} \rightarrow -NH_2Cd^{2+} \tag{12}$$

$$-NH_2 + OH^{-} \rightarrow -NH_2OH^{-} \tag{13}$$

$$-NH_2OH^{-} + Cd^{2+} \rightarrow -NH_2OH^{-}Cd^{2+} \tag{14}$$

$$-NH_2OH^{-} + CdOH^{+} \rightarrow -NH_2OH^{-}CdOH^{+} \tag{15}$$

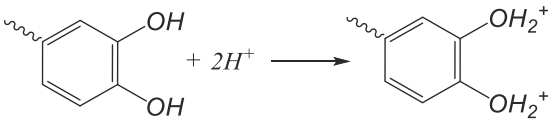

(16)

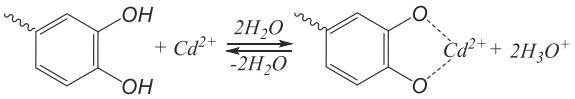

(17)

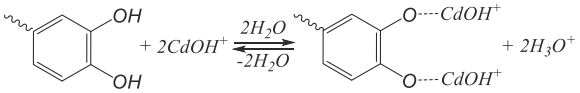

(18)

To verify the occurrence of ion exchange, the pH of the residual solutions at pH 6, 7, and 8 was measured after the completion of the experiment. The result revealed that the solution pH slightly decreases after adsorption, confirming the presence of the proposed mechanism for (17) and (18). This result indicated that the reactions of (17) and (18) considerably contribute to the overall adsorption process.

Reusability and Stability Studies

The reusability and stability of adsorbents are crucial for the industrial treatment of heavy metal wastewater. The inhibition of the heavy metal adsorption on Fe_3O_4@PDA at low pH indicated that acid treatment is a viable method for regenerating heavy metal-loaded adsorbents. Hence, in this experiment, 0.5 M HCl is used as the desorbent, and 10 adsorption–desorption cycles are carried out using the Fe_3O_4@PDA adsorbent. With the increase in the number of experiments, the adsorption capacity gradually decreased (Fig. 7c), possibly related to the incomplete desorption of cadmium ions adsorbed on the adsorbent surface. After the completion of the 10th cycle, the adsorption capacity of the adsorbents was reduced from 6.25 to 4.25 mg/g, and the adsorption rate only decreased by 3.6% compared with that of the initial cycle, indicating that Fe_3O_4@PDA exhibits

good reusability and provides a basis for the practical applications of Fe_3O_4@PDA.

TEM images of the adsorbent were recorded after 10 adsorption–desorption cycles (Fig. 1e). After 10 desorption cycles of Fe_3O_4@PDA in an acidic environment of 0.5 M HCl, the PDA layer was preserved, but the Fe_3O_4 core was corroded. Although the Fe_3O_4@PDA core structure was damaged, the core–shell structure was complete, and the adsorption efficiency did not change considerably, indicating that PDA exhibits a good protective effect on the Fe_3O_4 core and that Fe_3O_4@PDA can stably exist in an acidic environment. The results showed that Fe_3O_4@PDA exhibits excellent stability and adsorption properties, providing the basis for the practical applications of Fe_3O_4@PDA because if the adsorbent exhibits good reusability and stability, it will effectively decrease the cost of industrial applications.

Conclusions

In conclusion, a highly stable, hydrophilic functionalized magnetic nano-adsorbent (Fe_3O_4@PDA) was synthesized by a simple, safe, and environmentally friendly method in this study. Results revealed that the Cd^{2+} adsorption is dependent on the contact time, initial Cd^{2+} concentration, temperature, adsorbent dose, and solution pH. The adsorption performance of Cd^{2+} on Fe_3O_4@PDA was better than that of bare Fe_3O_4, which was related to the presence of active sites such as phenolic hydroxyl groups (electron negative groups) and amino groups on the Fe_3O_4@PDA surface. In kinetics studies, adsorption equilibrium was achieved at 120 min, and the adsorption capacity of Cd^{2+} onto Fe_3O_4@PDA reached up to 9.176 mg/g. The adsorption of Cd^{2+} followed the pseudo-second-order kinetics model. The adsorption of Cd^{2+} onto Fe_3O_4@PDA was consistent with the Freundlich isotherm, and the maximum adsorption capacity obtained by the Langmuir model was 21.58 mg/g. Thermodynamic analyses indicated that the reaction is spontaneous and endothermic. Meanwhile, the possible adsorption mechanism was also proposed on the basis of the kinetics, D-R isotherm model, and thermodynamic results, i.e., Cd^{2+} was adsorbed on the Fe_3O_4@PDA surface-active site by electrostatic adsorption, ion exchange, and chelation. Furthermore, 10 adsorption–desorption cycles were carried out using the Fe_3O_4@PDA nano-adsorbent for water samples containing cadmium. The adsorption rate of the adsorbent was only decreased by 3.6%, indicating that Fe_3O_4@PDA exhibits good adsorption stability and reusability, thereby reducing costs. The dissolution of Fe_3O_4@PDA in 0.5 M HCl indicated that the adsorbent can be treated harmlessly, avoiding secondary environmental pollution. The results revealed that Fe_3O_4@PDA exhibit immense potential for the treatment of cadmium-containing wastewater.

Abbreviations

BET: Brunauer–Emmet–Teller measurements; Fe_3O_4: $FeO{\cdot}Fe_2O_3$; Fe_3O_4@PDA: Fe_3O_4 modified with polydopamine; FTIR: Fourier transform infrared spectroscopy; TEM: Transmission electron microscopy; VSM: Vibrating sample magnetometer; XPS: X-ray photoelectron spectroscopy; XRD: X-ray diffraction

Acknowledgments

The authors acknowledge the Advanced Analysis and Measurement Center of Yunnan University.

Authors' Contributions

This study was carried out in collaboration of all the authors. TL designed the study, conducted experiments and analysis, and prepared the manuscript. FJ and XJY revised the manuscript. SJL, ZXR, and LLW played a part in the experimental process. LHT and SXW provided advice for the experimental design and participated in the revision of the manuscript. All authors read and approved the final manuscript.

Funding

This study was supported by the Natural Science Foundation of Yunnan Province (project no. 2018FB014), Scientific Research Foundation of Yunnan Provincial Department of Education (project no. 2018JS005), Natural Science Foundation of Yunnan University (project no. 2017YDQN01), and Major Project of Kunming Science and Technology Bureau (project no. 2017-1-S-12305).

Availability of Data and Materials

All data supporting the conclusions of this article are included within the article.

Competing Interests

The authors declare that they have no competing interests.

Received: 4 May 2019 Accepted: 9 September 2019
Published online: 28 November 2019

References

1. Salah TA, Mohammad AM, Hassan MA et al (2014) Development of nano-hydroxyapatite/chitosan composite for cadmium ions removal in wastewater treatment [J]. J Taiwan Inst Chem Eng 45(4):1571–1577. https://doi.org/10.1016/j.jtice.2013.10.008
2. Zhen ZY, En FL, En LZ et al (2017) Spatio-temporal variations, contamination and potential ecological risk of heavy metals in the sediments of Chenghai Lake [J]. Environ Sci 38(10):4169–4177. https://doi.org/10.13227/j.hjkx.201702131
3. Sharma YC (2008) Thermodynamics of removal of cadmium by adsorption on an indigenous clay [J]. Chem Eng J 145(1):64–68. https://doi.org/10.1016/j.cej.2008.03.006
4. Jafarnejadi AR, Sayyad G, Homaee M et al (2013) Spatial variability of soil total and DTPA-extractable cadmium caused by long-term application of phosphate fertilizers, crop rotation, and soil characteristics [J]. Environ Monit Assess 185(5):4087–4096. https://doi.org/10.1007/s10661-012-2851-2
5. Goering PL, Waalkes MP, Klaassen CD (1995) Toxicology of cadmium [J]. Handb Exp Pharmacol 115:189–214. https://doi.org/10.1007/978-3-642-79162-8_9
6. Mahalik MP, Hitner HW, Prozialeck WC (1995) Teratogenic effects and distribution of cadmium (Cd^{2+}) administered via osmotic minipumps to gravid CF-1 mice [J]. Toxicol Lett (Shannon) 76(3):195–202. https://doi.org/10.1016/0378-4274(95)80003-V
7. Organization W H. Health risks of heavy metals from long-range transboundary air pollution [J]. 2007
8. Vainio H, Heseltine E (1993) Meeting of the IARC working group on beryllium, cadmium, mercury and exposures in the glass manufacturing industry [J]. Scand J Work Environ Health 19(5):4. https://doi.org/10.5271/sjweh.1461
9. Guston DH (2005) Institutional design for socially robust knowledge: the National Toxicology Program's Report on Carcinogens [M]. Democratization Expertise:63–79. https://doi.org/10.1007/1-4020-3754-6_4
10. Bulut VN, Demirci H, Ozdes D et al (2016) A novel carrier element-free co-precipitation method for separation/preconcentration of lead and cadmium

ions from environmental matrices [J]. Environ Prog Sustain Energy 35(6): 1709–1715. https://doi.org/10.1002/ep.12422
11. Wong CW, Barford JP, Chen G et al (2014) Kinetics and equilibrium studies for the removal of cadmium ions by ion exchange resin [J]. J Environ Chem Eng 2(1):698–707. https://doi.org/10.1016/j.jece.2013.11.010
12. Kumar PR, Swathanthra PA, Rao VVB et al (2014) Adsorption of cadmium and zinc ions from aqueous solution using low cost adsorbents [J]. J Appl Sci 14(13):159–159. https://doi.org/10.3923/jas.2014.1372.1378
13. Li Y, Yang L, Xu Z et al (2017) Separation and recovery of heavy metals from waste water using synergistic solvent extraction [J]. IOP Conference Series: Materials Science and Engineering 167:012005 https://doi.org/2017.10.1088/1757-899X/167/1/012005
14. Meng Q, Nan J, Wang Z et al (2019) Study on the efficiency of ultrafiltration technology in dealing with sudden cadmium pollution in surface water and ultrafiltration membrane fouling [J]. Environ Sci Pollut Res 26(16):16641–16651. https://doi.org/10.1007/s11356-019-04691-4
15. Xu M, Mckay G (2017) Removal of heavy metals, lead, cadmium, and zinc, using adsorption processes by cost-effective adsorbents [J]. https://doi.org/10.1007/978-3-319-58136-1_5
16. Mahatantila K, Vithanage M, Seike Y et al (2012) Adsorptive removal of cadmium by natural red earth: equilibrium and kinetic studies [J]. Environ Technol 33(5):597–606. https://doi.org/10.1080/09593330.2011.586059
17. Du HH, Chen WL, Cai P et al (2016) Cadmium adsorption on bacteria–mineral mixtures: effect of naturally occurring ligands [J]. Eur J Soil Sci 67(5): 641–649. https://doi.org/10.1111/ejss.12373
18. Bhatnagar A, Hogland W, Marques M et al (2013) An overview of the modification methods of activated carbon for its water treatment applications [J]. Chem Eng J 219(3):499–511. https://doi.org/10.1016/j.cej.2012.12.038
19. Araki S, Li T, Li K et al (2019) Preparation of zeolite hollow fibers for high-efficiency cadmium removal from waste water [J]. Sep Purif Technol 221: 393–398. https://doi.org/10.1016/j.seppur.2019.04.011
20. Javaheri F, Kheshti Z, Ghasemi S et al (2019) Enhancement of Cd^{2+} removal from aqueous solution by multifunctional mesoporous silica: equilibrium isotherms and kinetics study [J]. Sep Purif Technol 224:199–208. https://doi.org/10.1016/j.seppur.2019.05.017
21. Pandey S, Tiwari S (2015) Facile approach to synthesize chitosan based composite-characterization and cadmium (II) ion adsorption studies [J]. Carbohydr Polym 134:646–656. https://doi.org/10.1016/j.carbpol.2015.08.027
22. Rahman ML, Sarkar SM, Yusoff MM (2016) Efficient removal of heavy metals from electroplating wastewater using polymer ligands [J]. Front Environ Sci Eng 10(2):352–361. https://doi.org/10.1007/s11783-015-0783-0
23. Tang SC, Lo IM (2013) Magnetic nanoparticles: essential factors for sustainable environmental applications [J]. Water Res 47(8):2613–2632. https://doi.org/10.1016/j.watres.2013.02.039
24. Petosa AR, Jaisi DP, Quevedo IR et al (2010) Aggregation and deposition of engineered nanomaterials in aquatic environments: role of physicochemical interactions [J]. Environ Sci Technol 44(17):6532–6549. https://doi.org/10.1021/es100598h
25. Phenrat T, Kim HJ, Fagerlund F et al (2009) Particle size distribution, concentration, and magnetic attraction affect transport of polymer-modified Fe^0 nanoparticles in sand columns [J]. Environ Sci Technol 43(13):5079–5085. https://doi.org/10.1021/es900171v
26. Harris RA, van der Walt H, Shumbula PM (2015) Engineered inorganic/organic-core/shell magnetic Fe_xO_y nanoparticles with oleic acid and/or oleylamine as capping agents [J]. Curr Pharm Des 21(37). https://doi.org/10.2174/1381612821666150917092826
27. Mohamed H, Zeid A, Mohamed ETA et al (2017) One-step carbon coating and polyacrylamide functionalization of Fe_3O_4 nanoparticles for enhancing magnetic adsorptive-remediation of heavy metals [J]. Molecules 22(12):2074. https://doi.org/10.3390/molecules22122074
28. Siping J, Changlin M, Hui L et al (2018) A hydrothermal synthesis of Fe_3O_4@C hybrid nanoparticle and magnetic adsorptive performance to remove heavy metal ions in aqueous solution [J]. Nanoscale Res Lett 13(1): 178. https://doi.org/10.1186/s11671-018-2580-8
29. Zhao X, Liu S, Zhi T et al (2015) Synthesis of magnetic metal-organic framework (MOF) for efficient removal of organic dyes from water [J]. Sci Rep 5(11849). https://doi.org/10.1038/srep11849
30. Lee H, Dellatore SM, Miller WM et al (2007) Mussel-inspired surface chemistry for multifunctional coatings [J]. Science 318(5849):426–430. https://doi.org/10.1126/science.1147241
31. Lee H, Scherer NF, Messersmith PB (2006) Single-molecule mechanics of mussel adhesion [J]. Proc Natl Acad Sci U S A 103(35):12999–13003. https://doi.org/10.1073/pnas.0605552103
32. Farnad N, Farhadi K, Voelcker NH (2012) Polydopamine nanoparticles as a new and highly selective biosorbent for the removal of copper (II) ions from aqueous solutions [J]. Water Air Soil Pollut 223(6):3535–3544. https://doi.org/10.1007/s11270-012-1131-7
33. Zhang S, Zhang Y, Bi G et al (2014) Mussel-inspired polydopamine biopolymer decorated with magnetic nanoparticles for multiple pollutants removal [J]. J Hazard Mater 270(8):27–34. https://doi.org/10.1016/j.jhazmat.2014.01.039
34. Huang S, Yang L, Liu M et al (2013) Complexes of polydopamine-modified clay and ferric ions as the framework for pollutant-absorbing supramolecular hydrogels [J]. Langmuir 29(4):1238–1244. https://doi.org/10.1021/la303855t
35. Gao H, Sun Y, Zhou J et al (2012) Mussel-inspired synthesis of polydopamine-functionalized graphene hydrogel as reusable adsorbents for water purification [J]. ACS Appl Mater Interfaces 5(2):425–432. https://doi.org/10.1021/am302500v
36. Liu S, Li S, Niu H et al (2014) Facile synthesis of novel flowerlike magnetic mesoporous carbon for efficient chlorophenols removal [J]. Microporous Mesoporous Mater 200:151–158. https://doi.org/10.1016/j.micromeso.2014.08.046
37. Bao S, Li K, Ning P et al (2017) Highly effective removal of mercury and lead ions from wastewater by mercaptoamine-functionalised silica-coated magnetic nano-adsorbents: Behaviours and mechanisms [J]. Appl Surf Sci 393:457–466. https://doi.org/10.1016/j.apsusc.2016.09.098
38. Ge Y, Li Y, Zu B et al (2016) AM-DMC-AMPS multi-functionalized magnetic nanoparticles for efficient purification of complex multiphase water system [J]. Nanoscale Res Lett 11(1):217. https://doi.org/10.1186/s11671-016-1434-5
39. Bao SY, Tang LH, Li K et al (2015) Highly selective removal of Zn (II) ion from hot-dip galvanizing pickling waste with amino-functionalized Fe_3O_4@SiO_2 magnetic nano-adsorbent [J]. J Colloid Interface Sci 462:235–242. https://doi.org/10.1016/j.jcis.2015.10.011
40. Wang Y, Wang S, Niu H, et al. Preparation of polydopamine coated Fe_3O_4 nanoparticles and their application for enrichment of polycyclic aromatic hydrocarbons from environmental water samples [J]. J Chromatogr A, 2013, 1283(3):20–26. doi: https://doi.org/10.1016/j.chroma.2013.01.110
41. Shen M, Jia W, Lin C et al (2014) Facile synthesis of folate-conjugated magnetic/fluorescent bifunctional microspheres [J]. Nanoscale Res Lett 9(1): 558. https://doi.org/10.1186/1556-276X-9-558
42. Li W, Wu H (2017) Sodium citrate functionalized reusable Fe_3O_4@TiO_2, photocatalyst for water purification [J]. Chem Phys Lett 686:178–182. https://doi.org/10.1016/j.cplett.2017.08.046
43. Liu J, Sun Z, Deng Y et al (2010) Highly water-dispersible biocompatible magnetite particles with low cytotoxicity stabilized by citrate groups [J]. Angew Chem 48(32):5875–5879. https://doi.org/10.1002/anie.200901566
44. Liu X, Cao J, Li H et al (2013) Mussel-inspired polydopamine: a biocompatible and ultrastable coating for nanoparticles in vivo [J]. ACS Nano 7(10):9384–9395. https://doi.org/10.1021/nn404117j
45. Fu JW, Chen ZH, Wang MH et al (2015) Adsorption of methylene blue by a high-efficiency adsorbent (polydopamine microspheres): kinetics, isotherm, thermodynamics and mechanism analysis [J]. Chem Eng J 259:53–61. https://doi.org/10.1016/j.cej.2014.07.101
46. Liebscher J, Mrówczyński R, Scheidt HA et al (2013) Structure of polydopamine: a never-ending story?[J]. Langmuir. https://doi.org/10.1021/la4020288
47. Hong YH, Zi QS, Meng CHE (2009) The adsorption mechanisms of cadmium on crosslinked chitosan templated under microwave irradiation [J]. Polym Mater Sci Eng 25(1):75–78. https://doi.org/10.1115/MNHMT2009-18287
48. Zangmeister RA, Morris TA, Tarlov MJ (2013) Characterization of polydopamine thin films deposited at short times by autoxidation of dopamine [J]. Langmuir 29(27):8619–8628. https://doi.org/10.1021/la400587j
49. Chiang YC, Lee CY, Lee HC (2007) Surface chemistry of polyacrylonitrile- and rayon-based activated carbon fibers after post-heat treatment [J]. Mater Chem Phys 101(1):199–210. https://doi.org/10.1016/j.matchemphys.2006.03.007
50. Moulder JF, Chastain J, King RC (1963) Handbook of X-ray photoelectron spectroscopy: a reference book of standard spectra for identification and interpretation of XPS data [J]. Chem Phys Lett 99(1):7–10. https://doi.org/10.1016/0009-2614(83)80259-0
51. Ali RM, Hamad HA, Hussein MM et al (2016) Potential of using green adsorbent of heavy metal removal from aqueous solutions: adsorption

kinetics, isotherm, thermodynamic, mechanism and economic analysis [J]. Ecol Eng 91:317–332. https://doi.org/10.1016/j.ecoleng.2016.03.015
52. Kiruba UP, Kumar PS, Prabhakaran C et al (2014) Characteristics of thermodynamic, isotherm, kinetic, mechanism and design equations for the analysis of adsorption in Cd (II) ions-surface modified eucalyptus seeds system [J]. J Taiwan Inst Chem Eng 45(6):2957–2968. https://doi.org/10.1016/j.jtice.2014.08.016
53. Ho YS (2006) Review of second-order models for adsorption systems [J]. J Hazard Mater 136(3):681–689. https://doi.org/10.1016/j.jhazmat.2005.12.043
54. Chen H, Dai G, Zhao J et al (2010) Removal of copper (II) ions by a biosorbent—cinnamomum camphora leaves powder [J]. J Hazard Mater 177(1–3):228–236. https://doi.org/10.1016/j.jhazmat.2009.12.022
55. Yang C (1998) Statistical mechanical study on the freundlich isotherm equation [J]. J Colloid Interface Sci 208(2):379–387. https://doi.org/10.1006/jcis.1998.5843
56. Zhang H, Niu Z, Liu Z et al (2015) Equilibrium, kinetic and thermodynamic studies of adsorption of Th (IV) from aqueous solution onto kaolin [J]. J Radioanalytical Nucl Chem 303(1):87–97. https://doi.org/10.1007/s10967-014-3324-6
57. Boparai HK, Joseph M, O'Carroll DM (2011) Kinetics and thermodynamics of cadmium ion removal by adsorption onto nano zerovalent iron particles [J]. J Hazard Mater 186(1):458–465. https://doi.org/10.1016/j.jhazmat.2010.11.029
58. Javadian H (2014) Application of kinetic, isotherm and thermodynamic models for the adsorption of Co (II) ions on polyaniline/polypyrrole copolymer nanofibers from aqueous solution [J]. J Ind Eng Chem 20(6):4233–4241. https://doi.org/10.1016/j.jiec.2014.01.026
59. Unlü N, Ersoz M (2006) Adsorption characteristics of heavy metal ions onto a low cost biopolymeric sorbent from aqueous solutions [J]. J Hazard Mater 136(2):272–280. https://doi.org/10.1016/j.jhazmat.2005.12.013
60. Xu R, Zhou G, Tang Y et al (2015) New double network hydrogel adsorbent: highly efficient removal of Cd (II) and Mn (II) ions in aqueous solution [J]. Chem Eng J 275:179–188. https://doi.org/10.1016/j.cej.2015.04.040
61. Kołodyńska D, Bąk J, Kozioł M et al (2017) Investigations of heavy metal ion sorption using nanocomposites of iron-modified biochar [J]. Nanoscale Res Lett 12(1). https://doi.org/10.1186/s11671-017-2201-y
62. Vuković GD, Marinković AD, Čolić M et al (2010) Removal of cadmium from aqueous solutions by oxidized and ethylenediamine-functionalized multi-walled carbon nanotubes [J]. Chem Eng J 157(1):238–248. https://doi.org/10.1016/j.cej.2009.11.026
63. Taty-Costodes VC, Fauduet H, Porte C et al (2003) Removal of Cd (II) and Pb (II) ions, from aqueous solutions, by adsorption onto sawdust of Pinus sylvestris [J]. J Hazard Mater 105(1–3):121–142. https://doi.org/10.1016/j.jhazmat.2003.07.009
64. Meena AK, Kadirvelu K, Mishraa GK et al (2008) Adsorption of Pb (II) and Cd (II) metal ions from aqueous solutions by mustard husk [J]. J Hazard Mater 150(3):619–625. https://doi.org/10.1016/j.jhazmat.2007.05.011
65. Liang S, Guo XY, Feng NC et al (2009) Adsorption of Cu^{2+} and Cd^{2+} from aqueous solution by mercapto-acetic acid modified orange peel [J]. Colloids Surf B Biointerfaces 73(1):10–14. https://doi.org/10.1016/j.colsurfb.2009.04.021
66. Hadavifar M, Bahramifar N, Younesi H et al (2014) Adsorption of mercury ions from synthetic and real wastewater aqueous solution by functionalized multi-walled carbon nanotube with both amino and thiolated groups [J]. Chem Eng J 237(2):217–228. https://doi.org/10.1016/j.cej.2013.10.014
67. Nagy B, Mânzatu C, Măicăneanu A et al (2014) Linear and nonlinear regression analysis for heavy metals removal using Agaricus bisporus, macrofungus [J]. Arab J Chem 10(S2):S3569–S3579. https://doi.org/10.1016/j.arabjc.2014.03.004
68. Lai CH, Chen CY, Wei BL et al (2002) Cadmium adsorption on goethite-coated sand in the presence of humic acid [J]. Water Res 36(20):4943–4950. https://doi.org/10.1016/S0043-1354(02)00009-X
69. Sánchez PM, Rivera UJ (2002) Adsorbent-adsorbate interactions in the adsorption of Cd (II) and Hg (II) on ozonized activated carbons [J]. Environ Sci Technol 36(17):3850–3854. https://doi.org/10.1021/es0255610
70. Hua Y, Xiao J, Zhang Q et al (2018) Facile synthesis of surface-functionalized magnetic nanocomposites for effectively selective adsorption of cationic dyes [J]. Nanoscale Res Lett 13(1):99. https://doi.org/10.1186/s11671-018-2476-7

Publisher's Note